Journal of Solid State Chemistry 183 (2010) 2869–2876

Contents lists available at ScienceDirect

Journal of Solid State Chemistry

journal homepage: www.elsevier.com/locate/jssc

Porous α-Fe_2O_3 hollow microspheres and their application for acetone sensor

Shurong Wang*, Liwei Wang, Taili Yang, Xianghong Liu, Jun Zhang, Baolin Zhu, Shoumin Zhang, Weiping Huang, Shihua Wu

Key Laboratory of Advanced Energy Materials Chemistry (MOE), Department of Chemistry, Nankai University, Tianjin 300071, China

ARTICLE INFO

Article history:
Received 14 May 2010
Received in revised form
8 September 2010
Accepted 27 September 2010
Available online 1 October 2010

Keywords:
Acetone sensor
α-Fe_2O_3 hollow microspheres
Synthesis
Characterization

ABSTRACT

Porous α-Fe_2O_3 hollow microspheres were synthesized through a simple and efficient carbon sphere template method. The samples were characterized by X-ray diffraction, X-ray photoelectron spectroscopy, scanning electron microscopy, transmission electron microscopy and N_2 adsorption–desorption. Structural characterization indicated that as-prepared α-Fe_2O_3 hollow microspheres had porous structure with around 200 nm in diameter and thin shell about 10 nm thick. The average pore size and Brunauer–Emmett–Teller specific surface area of α-Fe_2O_3 hollow microspheres were 6.5 nm and 111.6 m^2/g, respectively. The gas sensing behavior investigation showed that as-synthesized α-Fe_2O_3 hollow microspheres exhibited very good gas sensing property to acetone vapor.

1. Introduction

As an environmentally friendly n-type semiconductor, α-Fe_2O_3 has been proven to be a good gas sensitive material for detection of toxic, combustible, explosive and harmful gases in both domestic and industrial applications. Extensive studies have been done to improve the gas sensing performances of the α-Fe_2O_3 based sensor, such as adding promoters, doping additives, decreasing grain size, controlling pore and surface defects, etc. [1]. It is well-known that the shape and size of α-Fe_2O_3 have a significant influence on its gas sensing properties. α-Fe_2O_3 nanostructures with different morphologies have been successfully synthesized, including nanorods [2,3], nanotubes [4], nanowires [5] and hollow microspheres [6–8]. Some recent research has indicated that using carbon microspheres as templates to synthesize hollow microspheres is a simple but efficient approach. Up-to-date, several metal oxides, including WO_3, Ga_2O_3, SnO_2, TiO_2, had been fabricated through carbon sphere template process [9,10]. As a novel green template, in comparison with polymer or silica microspheres, carbon microspheres have one apparent feature: there are a number of hydroxyl groups (–OH) on the surface, which makes surface modification unnecessary.

As a chemical reagent, acetone is extensively applied in industry, but its easy volatilization and toxic nature make it dangerous to people at high concentration in air. It may cause a headache, fatigue, nausea, even narcosis and death with the concentration of acetone in air higher than 1000 ppm. High concentration acetone vapor will also have a bad influence on the function of kidney and liver. Thus, detecting and measuring acetone in the workplace is necessary for human's safety and health. In addition, acetone has been related to diabetes. The medical reports show that the average concentration of acetone in the breath products exhaled by diabetic patients and their blood is higher than that of healthy people [11,12]. The validity of acetone detection for diabetes diagnostics has been supported by extensive medical researches [13,14]. Therefore, sensor may be one of the most promising methods in measuring the concentration of acetone, due to its simplicity, precision and convenience.

In this paper, we develop a simple and efficient template approach to fabricate α-Fe_2O_3 hollow microspheres using carbon microspheres as templates and investigate the gas sensing behavior of the α-Fe_2O_3 hollow microspheres towards acetone vapor.

2. Experimental

All chemicals in this work were of analytical grade and were used as received without further purification.

2.1. Preparation of carbon microspheres

Carbon microspheres were prepared in a typical procedure. 7.2 g glucose was dissolved in 80 ml distilled water to get a clear solution and then hydrothermal treatment at 160 °C for 6 h. The precipitate was centrifuge-rinsed with distilled water and ethanol

* Corresponding author. Fax: +86 22 23502458.
E-mail address: shrwang@nankai.edu.cn (S. Wang).

0022-4596/$ - see front matter © 2010 Elsevier Inc. All rights reserved.
doi:10.1016/j.jssc.2010.09.033

for several times till getting the clear solution, and then dried at 80 °C in air for 12 h.

2.2. Preparation of porous α-Fe_2O_3 hollow microspheres

The synthesis process of porous α-Fe_2O_3 hollow microspheres was as follows: 0.5030 g carbon microspheres were uniformly dispersed in 100 ml N,N-dimethylformamide (DMF) by ultrasonication for 1 h. 0.1610 g $Fe(NO_3)_3 \cdot 9H_2O$ dissolved in 20 ml DMF was slowly dropped into the above mixture and then 20 drops of distilled water were added, followed by ultrasonication for 1 h. The mixed solution was aged under ambient temperature for 24 h. The resulting precursor was centrifugated and washed with distilled water and ethanol, then dried at 80 °C in air for 12 h. After calcined at 450 °C in air for 2 h, the product was cooled to room temperature, and red α-Fe_2O_3 powders were obtained.

2.3. Sample characterization

X-ray diffraction (XRD) measurement was performed on a Rigaku D/max-2500 diffractometer, with Cu $K\alpha$ radiation at 40 kV and 100 mA in a scanning range 3–80° (2θ). The diffraction peaks of the crystalline phase were compared with those of standard compounds reported in the JCPDS Date File. X-ray photoelectron spectroscopy (XPS) measurements were performed on a Kratos Axis Ultra DLD spectrometer with the Al $K\alpha$ X-ray source ($h\nu$=1486.6 eV), hybrid (magnetic/electrostatic) optics and a multi-channel plate and delay line detector (DLD). In order to subtract the surface charging effect, the C1s peak was fixed, in agreement with the literature, at a binding energy of 284.6 eV. Scanning electron microscopy (SEM, Shimadzu SS-550, 15 kV) and high-resolution transmission electron microscopy (HRTEM, Philips FEI Tecnai 20ST, 200 kV) were carried out to observe the morphologies of the sample. Nitrogen adsorption–desorption isotherms were collected at liquid nitrogen temperature using a Quantachrome NOVA 2000e sorption analyzer. The specific surface area (S_{BET}) of the sample was calculated following the multi-point Brunauer–Emmett–Teller (BET) procedure. The pore-size distribution was determined from the adsorption branch of the isotherms using the Barett–Joyner–Halenda (BJH) method.

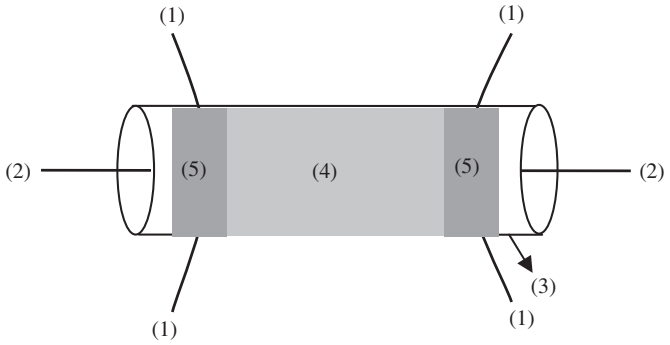

Scheme 1. Schematic diagram of the α-Fe_2O_3 hollow sphere based sensor: (1) Pt wire; (2) Ni–Cr heated wire; (3) Al_2O_3 tube; (4) sensing film; and (5) Au electrode.

2.4. Fabrication of the gas sensor and measurement of the sensing performance

Alumina substrate tube 4 mm long was used for the heater and sensing base. α-Fe_2O_3 hollow sphere powders were mixed with distilled water, and then were coated onto alumina tube attached with Pt electrodes. The schematic diagram of a typical gas sensor is shown in Scheme 1. The gas sensing behavior was investigated by using the commercial gas-sensing measurement system of HW-30A. The sensor signal was recorded by a computer at a constant test voltage of 5 V. The operating temperature was controlled by tuning the heating voltage. The sensor response was calculated as the ratio R_{air}/R_{vap}, where R_{air} and R_{vap} are the resistance values of the sample in air and in the presence of acetone vapor, respectively. The response and recovery times were obtained by the time for 90% of full response or 90% of full recovery of the response.

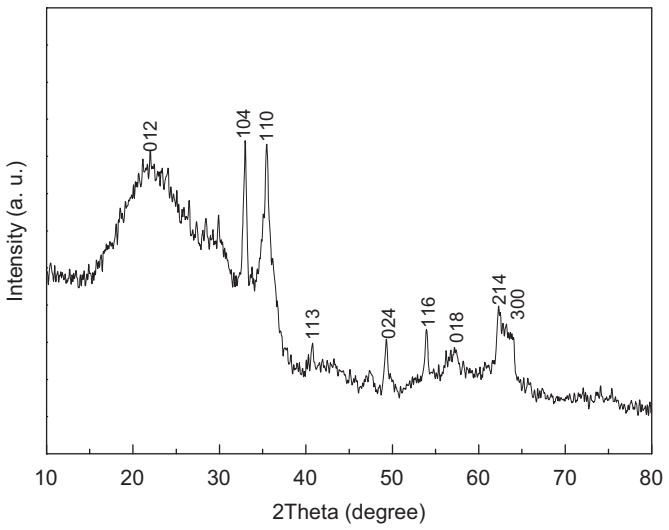

Fig. 1. XRD pattern of the as-prepared α-Fe_2O_3 hollow microspheres.

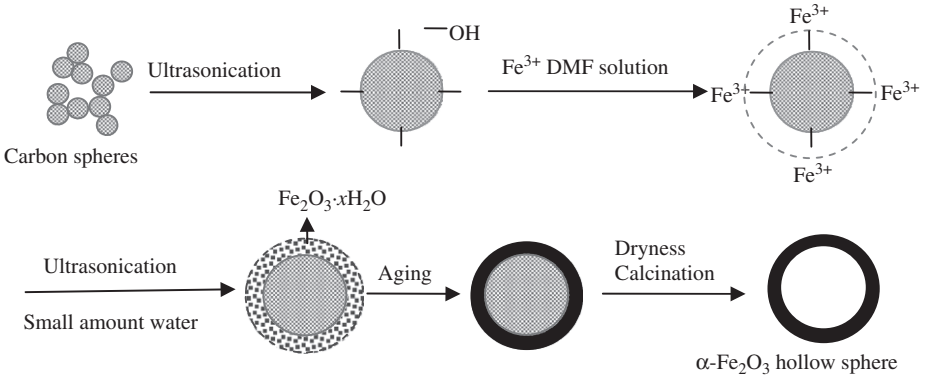

Scheme 2. Schematic illustration of the formation process of α-Fe_2O_3 hollow microspheres.

3. Results and discussion

A rational mechanism of the formation of α-Fe_2O_3 hollow microspheres is described in Scheme 2. Because as-prepared carbon microspheres had plenty of hydroxyl groups (–OH) on the surface, Fe^{3+} cations can be absorbed onto the surface of carbon microspheres and bind to the surface hydroxyl groups. Then Fe^{3+} further hydrolyzed to form $Fe_2O_3 \cdot xH_2O$ shell on the surface of the carbon microspheres, the presence of small amount water can promote the hydrolysis reaction, forming a core–shell structure. During calcination the aggregation of Fe_2O_3 nanoparticles resulted in the formation of the pores in shell and the carbon microspheres were removed in the form of carbon dioxide which could escape through the pores [15].

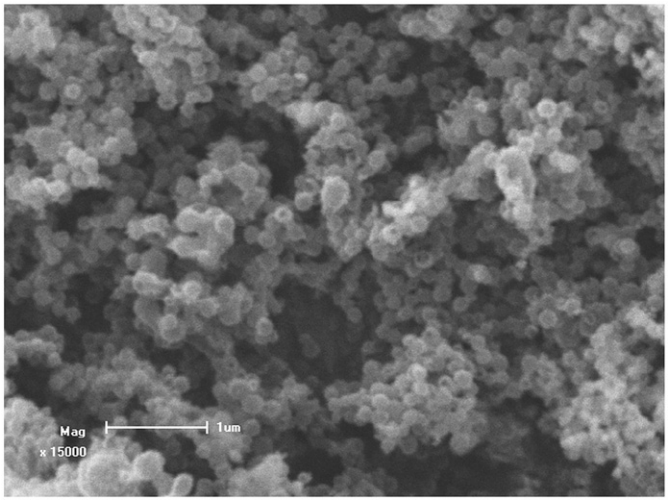

Fig. 2. SEM of α-Fe_2O_3 hollow microspheres.

XRD was used to identify the crystal phase of the sample. Fig. 1 shows the XRD pattern of the as-prepared product. It is clear that all the diffraction peaks in the XRD pattern can be readily indexed as α-Fe_2O_3 (JCPDS file no. 33–664), and size-broadening of the reflection peaks can be observed. No characteristic reflection peaks from other Fe species can be detected in the sample. The mean crystallite size is 6.7 nm, determined using Scherrer's equation from (110) diffraction peak of α-Fe_2O_3.

SEM analyses were performed to examine the morphology of the sample. Fig. 2 shows the SEM images of as-prepared α-Fe_2O_3 hollow microspheres. As shown, SEM overview observation reveals that as-prepared α-Fe_2O_3 products consist of spherical microstructures with the diameter of around 200 nm. The outer surfaces of the microspheres are rough, indicating that they are composed of a large number of loosely packed nanoparticles. Close observation reveals that there is partial cave-in on the surface of some microspheres, indicating the hollow core of the sample and thin shell wall.

To further investigate the structure of α-Fe_2O_3 hollow microspheres, the sample was characterized by HRTEM. Fig. 3 displays the TEM images of the hollow microspheres and the electron diffraction pattern. The strong contrast between the dark edges and pale centers in these images confirms the hollow structure of the α-Fe_2O_3 microspheres, with thin shell about 10 nm thick. It can also be clearly observed that the shell is composed of a large

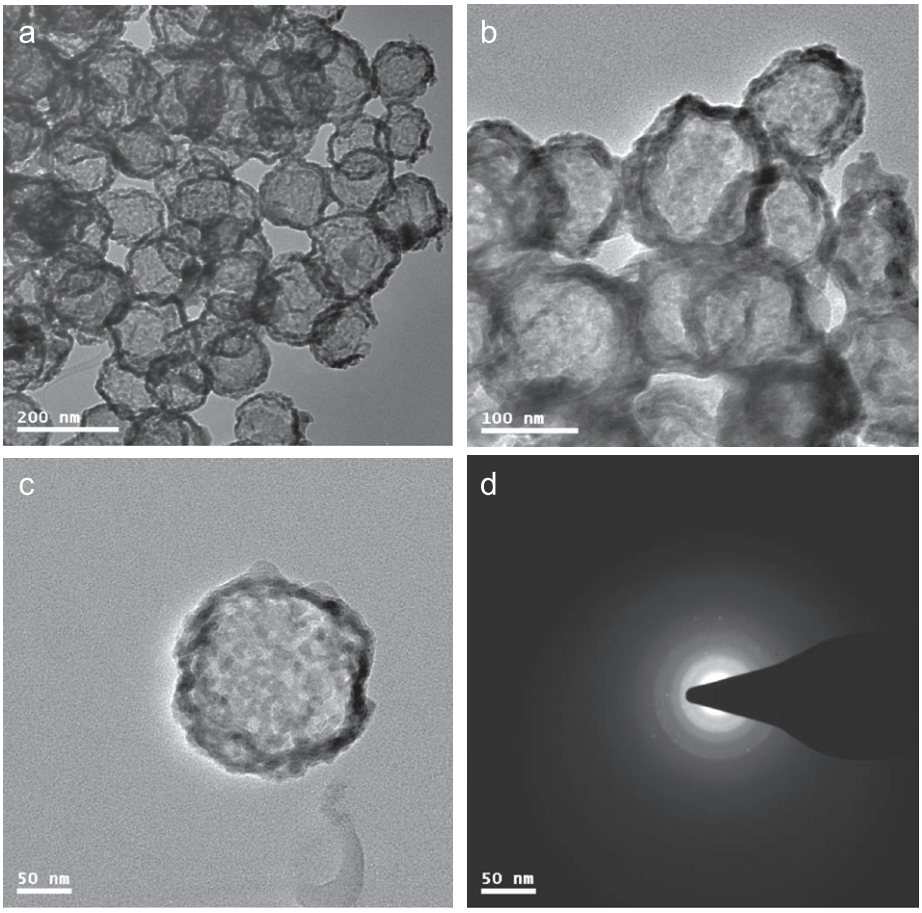

Fig. 3. HRTEM images (a–c) and SAED pattern (d) of α-Fe_2O_3 hollow microspheres.

number of very small nanoparticles and constitutes a porous framework. The corresponding selected area electron diffraction (SAED) pattern of α-Fe_2O_3 hollow microspheres further reveals that the hollow microspheres are composed of α-Fe_2O_3 polycrystallites.

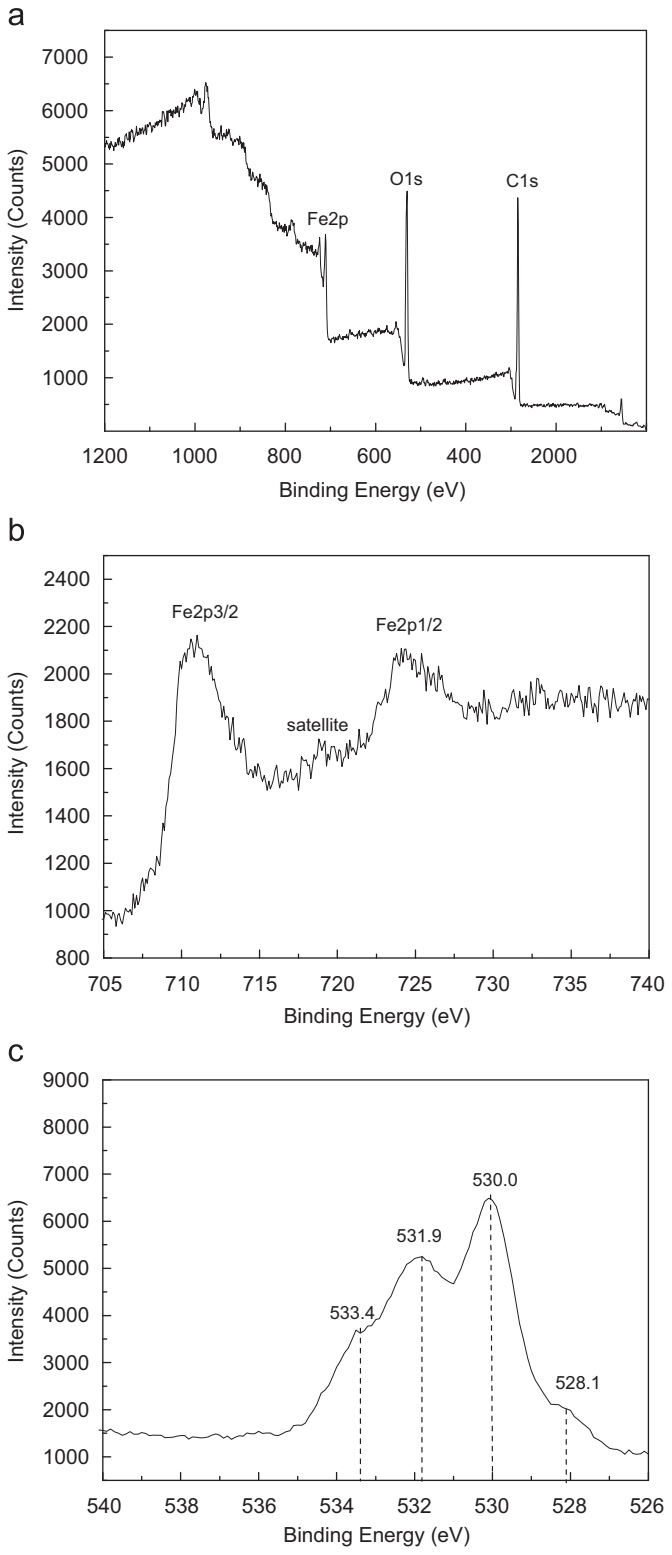

Fig. 4. XPS of α-Fe_2O_3 hollow microspheres: (a) full-range XPS spectrum, (b) Fe 2*p* and (c) O 1*s*.

XPS analysis was used to study the surface compositions of the product. As seen in Fig. 4a, the wide XPS picture of the product shows that no peaks of other elements except C, Fe and O were

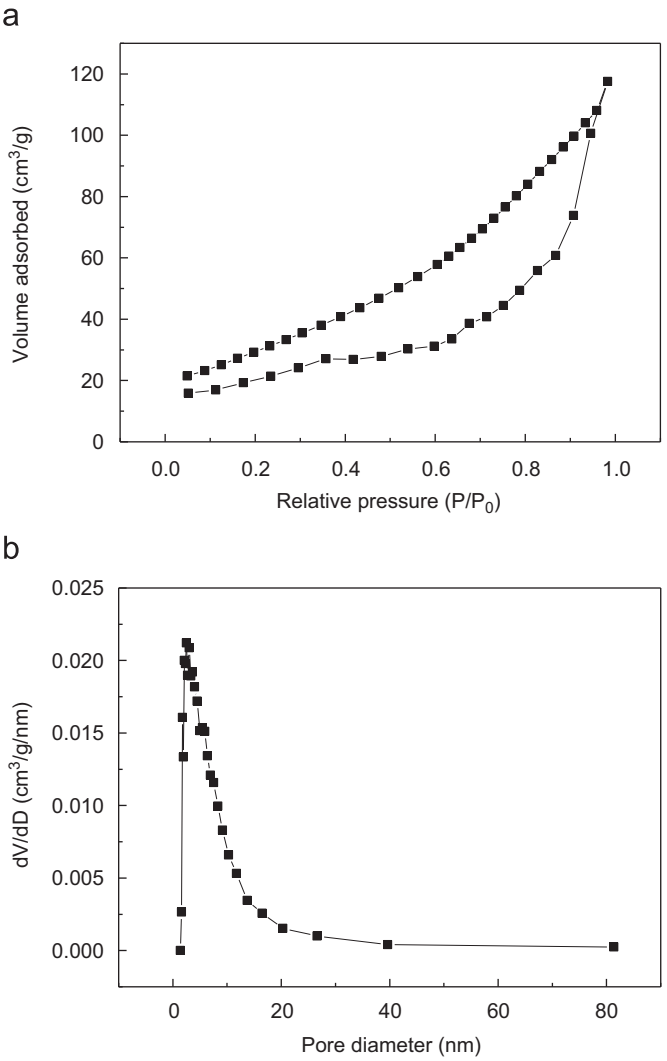

Fig. 5. N_2 adsorption–desorption isotherm (a) and BJH pore-size distribution plot (b) of hollow α-Fe_2O_3 microspheres.

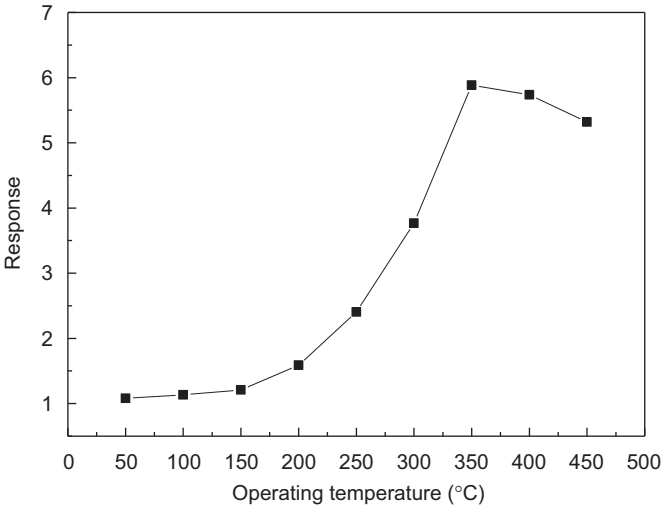

Fig. 6. Response of α-Fe_2O_3 hollow microspheres to 100 ppm acetone vapor at different operating temperatures.

observed in the picture, indicating that the product consists of Fe and O. The calculated atomic ratio of Fe and O by XPS is approximately 1:4, which is much lower than that (1:1.5) in α-Fe_2O_3, suggesting that as-prepared α-Fe_2O_3 hollow microspheres possess the excess oxygen and the enhanced oxygen adsorption capability. Fig. 4b shows the high-resolution XPS of Fe

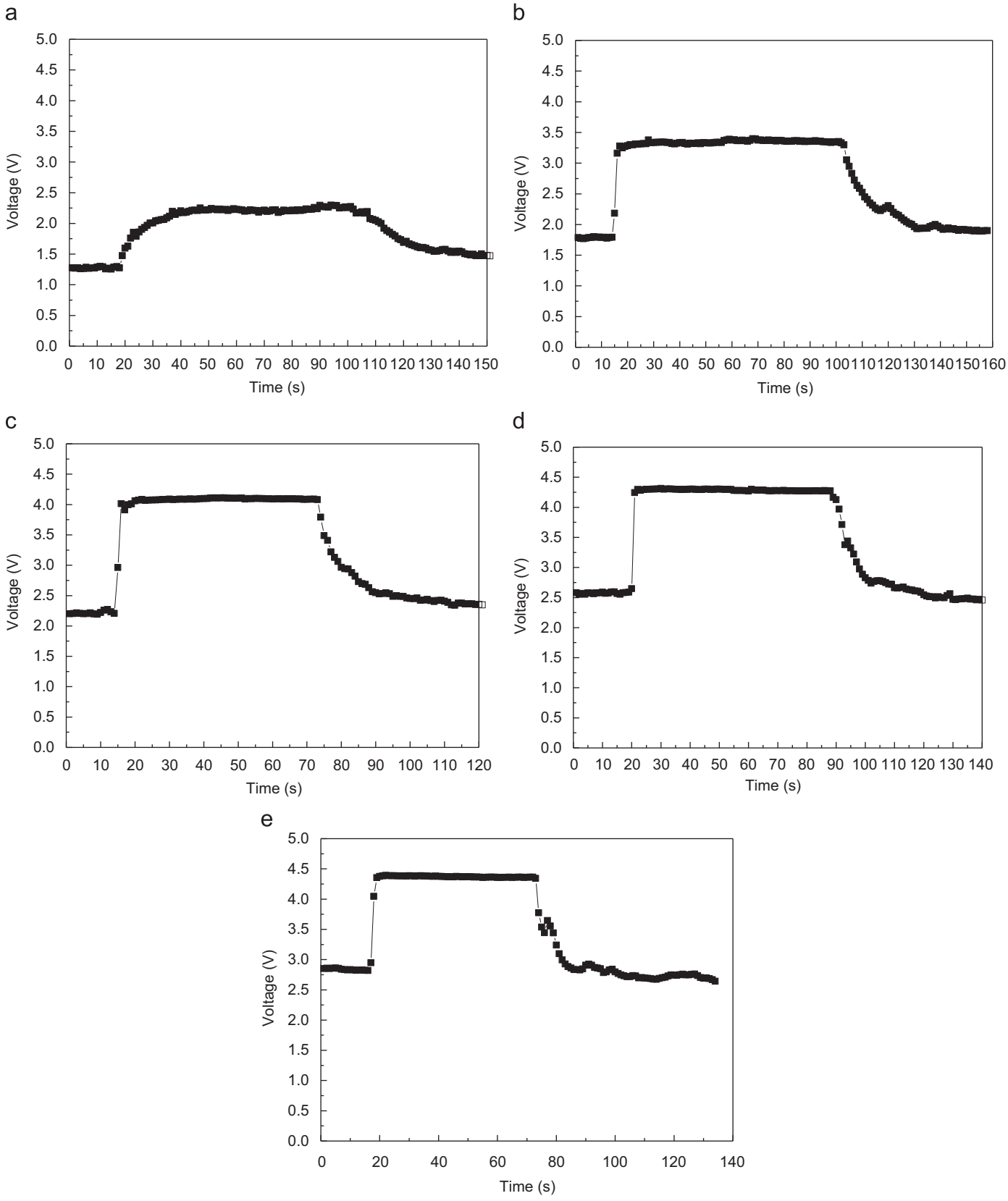

Fig. 7. Response and recovery characteristics curves of α-Fe_2O_3 to 100 ppm acetone vapor at different operating temperatures: (a) 250 °C, (b) 300 °C, (c) 350 °C, (d) 400 °C and (e) 450 °C.

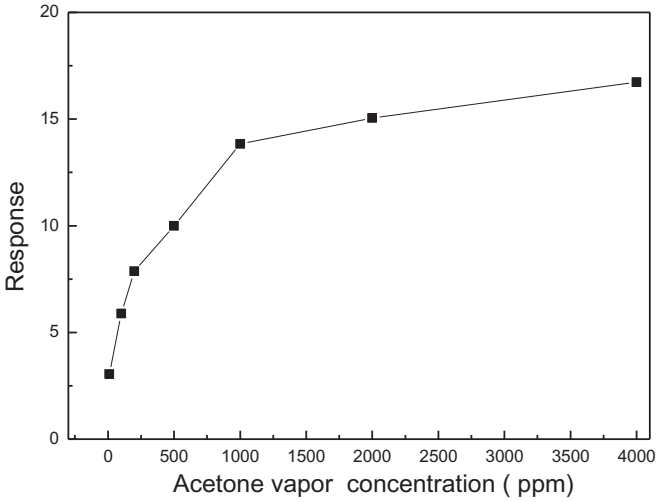

Fig. 8. Response of α-Fe_2O_3 hollow microspheres to different acetone vapor concentrations at the operating temperature of 350 °C.

2*p*. The binding energies of Fe $2p_{3/2}$ and Fe $2p_{1/2}$ are centered at 710.6 and 724.4 eV, respectively, with an energy separation between the spin–orbit doublet of 14 eV, indicating the existence of the oxidation state of Fe^{3+} [16]. As shown in Fig. 4c, the O 1*s* spectrum is broad, complex and exhibits four peaks. There exists two types of crystal lattice oxygen species on the sample, and the binding energies are 528.1 and 530.0 eV, respectively. Peak at 530.0 eV is in good agreement with crystal lattice oxygen in α-Fe_2O_3 bonded to Fe^{3+} [17]. The origin of peak at 528.1 eV is obscure. It is suggested that the peak at 528.1 eV may root in the crystal lattice oxygen bonded to both Fe^{3+} and H^+ (Fe–O–H). The different in electronegative between Fe^{3+} and H^+ influences their bonding state with O^{2-}, which results in the shift in O 1*s* energy level and the decrease in binding energies. As can be seen, there also exists two types of chemisorbed oxygen species. The binding energies are around 531.9 and 533.4 eV, respectively. It is well known that position of the signal of O 1*s* of the adsorbed oxygen relies on the charge state of adsorbed oxygen [18]. Peak at 531.9 eV is attributed to adsorbed O^- species on the surface of α-Fe_2O_3 hollow microspheres, and peak at 533.4 eV is attributed to chemisorbed O_2^- species on the surface.

The surface area and porosity of the α-Fe_2O_3 hollow microspheres were investigated by means of Brunauer–Emmett–Teller (BET) analysis and nitrogen adsorption and desorption isotherms. Because the α-Fe_2O_3 hollow microspheres are composed of a large number of nanoparticles, a high surface area can be expected, which is proven by BET analysis. The BET specific surface area is 111.6 m^2/g. Fig. 5a and b shows the N_2 adsorption–desorption isotherms and the corresponding pore size distribution of α-Fe_2O_3 hollow microspheres. A distinct hysteresis loop can be observed between adsorption and desorption branch, indicating porous structure of α-Fe_2O_3 hollow microspheres. The plot of the pore size distribution reveals that the porous hollow microspheres with a size distribution of 1–20 nm and centered at 2.5 nm. The α-Fe_2O_3 hollow microspheres have an average pore diameter of 6.5 nm.

Acetone gas sensing measurements were carried out at different operating temperatures and different acetone vapor concentrations in air.

To determine the optimal operating temperature to detect acetone vapor, the sensor working temperature was varied from 50 to 450 °C. As seen in Figs. 6 and 7, the operating temperature has a great influence on the acetone vapor response and on the dynamic behavior of the response. Fig. 6 reports the response of the sensor to 100 ppm acetone vapor as a function of operating temperature. The sensor response is observed to be poor when the operating temperature is below 200 °C, while the sensor response is very good when the operating temperature is above 250 °C, and the response reaches a maximum value at the operating temperature of 350 °C. However, the sensor response is observed to degrade when the operating temperature is higher than 400 °C.

As mentioned earlier, the α-Fe_2O_3 hollow microspheres are porous and possess a large amount of chemisorbed oxygen species (O_2^- and O^-) on the surface. The large specific surface and the increasing effective adsorption sites on the surface result in the improved sensing property. When the α-Fe_2O_3 hollow microspheres are exposed to the reducing gas like acetone vapor, the acetone vapor reacts with the chemisorbed oxygen species, which induces that the electrons are released back to the conduction band, accompanied with a decrease in resistance [19].

It is well known that the change in resistance of semiconducting oxide gas sensors is primarily caused by adsorption and desorption of gas molecules on the surface of the sensor [20]. Therefore, it is suggested that the sensing behavior of the sensor not only relies on the interaction of acetone vapor molecules with chemisorbed oxygen species, but rather on the adsorption of the acetone vapor molecules on the surface and the desorption of the products. At lower temperature, the reaction products do not get readily desorbed from the sensor surface. The species cover the sensing sites on the sensor surface, which prevents the further reaction between acetone vapor and chemisorbed oxygen. Subsequently, no appreciable change in the resistance of the sensor is observed, so the resistance of the sensor decreases little, resulting in the lower response. As increase in the operating temperature the reaction products are readily desorbed, giving sensing sites on the sensor to react with new gas species, resulting in the higher response. However, when the operating temperature is higher than the optimal temperature, the acetone is difficult to be adsorbed, resulting in less acetone vapor reacting with chemisorbed oxygen. Therefore, the response decreases.

Fig. 7 depicts the response and recovery characteristics curves versus operating temperature to 100 ppm acetone vapor. The response and recovery times are found to be dependent upon the operating temperature. The response times are very fast, lower than 5 s, at all operating temperature except 250 °C (17 s). In contrast, the recovery times are relatively long and become longer with increasing the operating temperature, however, the values of recovery times lie within 30 s.

Fig. 8 shows the response of α-Fe_2O_3 hollow microspheres based sensor as a function of the acetone vapor concentration at the optimal working temperature of 350 °C. As can be observed, the response increases significantly with increasing the acetone vapor concentration from 10 to 1000 ppm. The increase in the gas concentration implies a large surface coverage, resulting in an increase in the surface reaction between the surface adsorbed oxygen species and the vapor molecules. The chemisorbed negative oxygen ions on the sensor surface can react with acetone to release electrons, and with the increase in vapor concentrations more electrons may be released to the surface of sensor, resulting in an increase in response. However, the response slowly increases with increase in the acetone vapor concentrations above 1000 ppm, which indicates that the sensor response exhibits more or less saturation of the surface coverage of vapor molecules. The similar behavior has been observed by other groups [19,21].

Fig. 9 shows the response and recovery characteristic curves for different concentrations of acetone vapor at the operating temperature of 350 °C. As seen from Fig. 9, the response is very

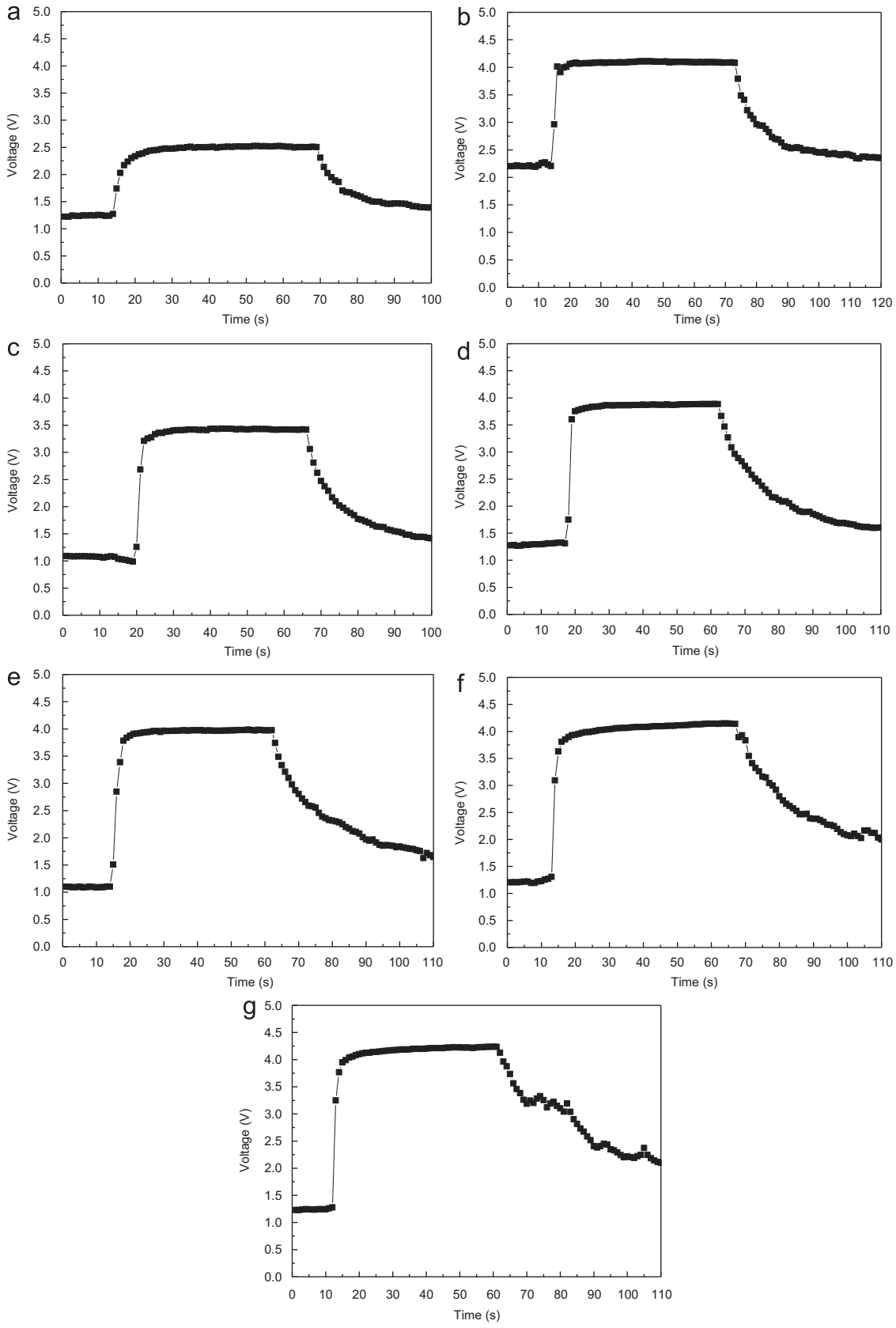

Fig. 9. Response and recovery characteristics curves of α-Fe_2O_3 to different concentrations of acetone vapor at the operating temperature of 350 °C: (a) 10 ppm, (b) 100 ppm, (c) 200 ppm, (d) 500 ppm, (e) 1000 ppm, (f) 2000 ppm and (g) 4000 ppm.

fast and the response times are within 5 s after exposed to different concentrations of acetone vapor. However, the recovery is not as quick as the response, and the recovery time increases with increasing acetone vapor concentrations. Fortunately, the recovery time does not exceed 30 s even the vapor concentrations up to 4000 ppm.

4. Conclusions

In summary, porous α-Fe_2O_3 hollow microspheres were synthesized through a simple and efficient carbon microsphere template method. The samples were characterized by XRD, XPS, SEM, TEM and N_2 adsorption–desorption. Structural characterization indicates that as-prepared α-Fe_2O_3 hollow microspheres have porous structure with around 200 nm in diameter and about 10 nm in shell thick. The average pore size and BET surface area of hollow microspheres are 6.5 nm and 111.6 m^2/g, respectively. The acetone gas sensing behavior investigation shows that as-synthesized α-Fe_2O_3 hollow microspheres exhibit very good response to acetone vapor.

Acknowledgments

This work was financially supported by the National Natural Science Foundation of China (No. 20871071) and Science and Technology Commission Foundation of Tianjin (Nos. 09JCYBJC03600 and 10JCYBJC03900).

References

[1] Y. Wang, J.L. Cao, S.R. Wang, X.Z. Guo, J. Zhang, H.J. Xia, S.M. Zhang, S.H. Wu, J. Phys. Chem. C 112 (2008) 17804–17808.
[2] B. Tang, G. Wang, L. Zhuo, J. Ge, L. Cui, Inorg. Chem. 45 (2006) 5196–5200.
[3] J.J. Wu, Y.L. Lee, H.H. Chiang, D.K.P. Wong, J. Phys. Chem. B 110 (2006) 18108–18111.
[4] C.J. Jia, L.D. Sun, Z.G. Yan, L.P. You, F. Luo, X.D. Han, Y.C. Pang, Z. Zhang, C.H. Yan, Angew. Chem. Int. Edn. 44 (2005) 4328–4331.
[5] L. Suber, P. Imperatori, G. Ausanio, F. Fabbri, H. Hofmeister, J. Phys. Chem. B 109 (2005) 7103–7109.
[6] Y.J. Xiong, Z.Q. Li, X.X. Li, B. Hu, Y. Xie, Inorg. Chem. 43 (2004) 6540–6542.
[7] D.H. Chen, D.R. Chen, X.L. Jiao, Y.T. Zhao, J. Mater. Chem. 13 (2003) 2266–2270.
[8] M.-M. Titirici, M. Antonietti, A. Thomas, Chem. Mater. 18 (2006) 3808–3812.
[9] R.A. Caruso, Top. Curr. Chem. 226 (2003) 91–118.
[10] X. Wang, P. Hu, Y. Fangli, L. Yu, J. Phys. Chem. C 111 (2007) 6706–6712.
[11] S.S. Likhodii, K. Musa, S.C. Cunnane, Clin. Chem. 48 (2002) 115–120.
[12] N. Makisimovich, V. Vorotyntsev, N. Nikitina, O. Kaskevich, P. Karabun, F. Martynenko, Sens. Actuator B 36 (1996) 419–421.
[13] O.E. Owen, V.E. Trapp, C.L. Skutches, M.A. Mozzoli, R.D. Hoeldtke, G. Boden, G.A. Reichard, Diabetes 31 (1982) 242–248.
[14] G.A. Reichard, C.L. Skutches, R.D. Hoeldtke, O.E. Owen, Diabetes 35 (1986) 668–674.
[15] J. Yu, X. Yu, B. Huang, X. Zhang, Y. Dai, Cryst. Growth Des. 9 (2009) 1474–1480.
[16] R. Zboril, M. Mashlan, Chem. Mater. 14 (3) (2002) 969–982.
[17] T.L. Barr, Modern ESCA: The Principles and Practice of X-ray Photo-electron Spectroscopy, CRC Press, Boca Raton, 1994.
[18] L. Hozer, Semiconductor Ceramics: Grain Boundary Effects Ellis Horwood, New York, 1994.
[19] R.S. Khadayate, J.V. Sali, P.P. Patil, Talanta 72 (2007) 1077–1081.
[20] T.J. Hsueh, C.L. Hsub, S.J. Changa, I.C. Chen, Actuators B: Chem. 126 (2007) 473–477.
[21] M.A. Henderson, J. Phys. Chem. B 109 (24) (2005) 12062–12070.